



### **JGR Space Physics**



#### RESEARCH ARTICLE

10.1029/2021JA029879

#### **Key Points:**

- Different forms of plasma depletions develop at midlatitudes in the absence of plasma bubbles in the equatorial region
- Plasma depletions develop locally in midlatitudes in association with traveling ionospheric disturbances
- Coincident occurrence of plasma depletions in midlatitudes and equatorial regions does not warrant their connection

#### Correspondence to:

J. Lee, jiyunlee@kaist.ac.kr

#### Citation:

Chang, H., Kil, H., Sun, A. K., Zhang, S.-R., & Lee, J. (2022). Ionospheric disturbances in low- and midlatitudes during the geomagnetic storm on 26 August 2018. *Journal of Geophysical Research: Space Physics*, 127, e2021JA029879. https://doi. org/10.1029/2021JA029879

Received 14 AUG 2021 Accepted 14 JAN 2022

# © 2022. The Authors. This is an open access article under the terms of the Creative Commons Attribution-NonCommercial-NoDerivs License, which permits use and distribution in any medium, provided the original work is properly cited, the use is non-commercial and no modifications or adaptations are made.

## **Ionospheric Disturbances in Low- and Midlatitudes During the Geomagnetic Storm on 26 August 2018**

Hyeyeon Chang<sup>1</sup>, Hyosub Kil<sup>2</sup>, Andrew K. Sun<sup>1</sup>, Shun-Rong Zhang<sup>3</sup>, and Jiyun Lee<sup>1</sup>

<sup>1</sup>Department of Aerospace Engineering, Korea Advanced Institute of Science and Technology, Daejeon, Korea, <sup>2</sup>Johns Hopkins University Applied Physics Laboratory, Laurel, MD, USA, <sup>3</sup>Haystack Observatory, Massachusetts Institute of Technology, Westford, MA, USA

**Abstract** Plasma density depletions at midlatitudes during geomagnetic storms are often understood in terms of equatorial plasma bubbles (EPBs) due to their morphological similarity. However, our study reports the observations that reveal the generation of plasma depletions at midlatitudes by local sources. During the geomagnetic storm on 26 August 2018, the Defense Meteorological Satellite Program and Swarm satellites detected plasma depletions at midlatitudes in the Asian sector in the absence of EPBs in the equatorial region. This observation and the total electron content (TEC) maps over Japan demonstrate that traveling ionospheric disturbances (TIDs) are the sources of midlatitude plasma depletions in the Asian sector. Near the west coast of the United States, the development of a narrow TEC depletion band was identified from TEC maps. The TEC depletion band, which is elongated in the northwest–southeast direction, moves toward the west with a velocity of approximately 240 m/s. The TEC at the TEC depletion band is about 5 TEC units ( $10^{16}$  m<sup>-2</sup>) smaller than the ambient TEC. As this band is confined to the midlatitudes, this phenomenon is not associated with an EPB. The characteristics of the TEC depletion band are consistent with those of medium-scale TIDs. Observations in the Asian sector and the TEC depletion band over the United States demonstrate that plasma depletions can develop at midlatitudes by local sources. Therefore, the morphological similarity between midlatitude irregularities and EPBs or their coincident occurrence does not provide corroborating evidence of their connection.

#### 1. Introduction

Plasma density irregularities in low-latitude and midlatitude F regions are normally understood in terms of equatorial plasma bubbles (EPBs) and traveling ionospheric disturbances (TIDs), respectively. Referring to the ground-based observations, such as total electron content (TEC) maps and all-sky airglow images, EPBs and TIDs can be distinguished by their propagation directions or alignments (Miller et al., 2009; Nishioka et al., 2008; Otsuka et al., 2012; Takahashi et al., 2018). As this information is not available from in situ satellite observations, EPBs and TIDs in the satellite observations are often distinguished by the occurrence latitudes and amplitude of electron density irregularities (Aa et al., 2020; Kil & Paxton, 2017; Kil et al., 2020; Lee et al., 2021; Park et al., 2010; Su et al., 2006). EPBs are mostly confined within  $\pm 25^{\circ}$  magnetic latitudes during magnetically quiet conditions (Aa et al., 2020; Kil & Heelis, 1998a; Kil et al., 2020; Su et al., 2006), and EPBs produce more intense irregularities than do TIDs (Kil et al., 2020).

During geomagnetic storms, large amplitude irregularities occur at midlatitudes as well as in the equatorial region. As the storm time midlatitude irregularities often appear as plasma depletions (or bubbles), EPBs have been suspected as their source (Aa et al., 2018, 2019; Cherniak & Zakharenkova, 2016; Cherniak et al., 2019; Huang et al., 2007; Ma & Maruyama, 2006; Martinis et al., 2015; Zakharenkova & Cherniak, 2020). In addition to morphological similarity, the coincident occurrence of midlatitude plasma depletions and EPBs at the same longitudes is provided as supporting evidence of their connection. However, this interpretation is effective when EPBs act as a unique source of midlatitude plasma depletions. As severe plasma depletions can develop in association with TIDs (Kil et al., 2016; Nishioka et al., 2009), the morphological similarity or the coincident occurrence of EPBs does not warrant the association of midlatitude plasma depletion with EPBs.

So far, the study on midlatitude plasma depletion has been focused on the demonstration of the role of EPBs. However, the growth of EPBs from the equator to midlatitudes is difficult to identify by observations due to sparse temporal and spatial coverage of observational data. Numerical simulations suggest that EPBs stop growing when the magnetic flux-tube-integrated ion mass density inside an EPB equals that of the EPB-embedded

CHANG ET AL. 1 of 11



background ionosphere (Krall et al., 2010; Mendillo et al., 2005). Based on the numerical calculation of the magnetic flux-tube integrated ion mass density, Mendillo et al. (2005) claimed that EPBs could grow beyond a magnetic apex height of 3,000 km, but, to the best of our knowledge, model simulations have not yet demonstrated the growth of EPBs to the magnetic apex height of several thousand kilometers. Because the upward motion of EPBs ceases when the ion mass density at the upper envelope of an EPB is approximately equal to that of the background ionosphere (Krall et al., 2010), EPBs would not grow indefinitely.

In addition to evaluating the relationship between midlatitude plasma depletions and EPBs, equal attention should be paid to local sources in the midlatitudes. The ionospheric observations during the geomagnetic storm on 26 August 2018 pave the way for diagnosing the source of midlatitude plasma depletions. From the observations of the Defense Meteorological Satellite Program (DMSP) and Swarm satellites during the storm, we identified the development of midlatitude plasma depletions in the absence of EPBs in the equatorial region. We also detected a TEC depletion band which was not related to an EPB. Using these observations, we discuss the roles of EPBs and TIDs in generating plasma depletions at midlatitudes.

#### 2. Data Description

Three Swarm satellites, named Alpha (A), Bravo (B), and Charlie (C), were launched on 22 November 2013, into near-circular orbits. Swarm-A and Swarm-C are pair satellites that fly side-by-side, maintaining a longitudinal distance of approximately 1.5°. Their orbital inclinations and altitudes were 87.5° and 470 km, respectively. Swarm-B is a standalone satellite with a slightly different orbital inclination (88°) and altitude (520 km). We use the measurements of the electron density by the Langmuir Probe instruments onboard Swarm-B and Swarm-C. The data cadence of the electron density is 0.5 s. Because Swarm-A and Swarm-C orbits were relatively close, we use only the Swarm-C data.

DMSP satellites comprise sun-synchronous near-circular orbits at an altitude of 840 km. This study uses the measurements of the ion density by the Special Sensor-Ions, Electrons, and Scintillation instruments onboard the DMSP F15, F16, and F17 satellites. The DMSP satellite orbits slowly drift with time, and the solar local times (LTs) at the descending nodes of the F15, F16, and F17 orbits on 26 August 2018 were 2.9, 3.8, and 6.6 hr, respectively. The data cadence of DMSP satellites was 1 s.

We investigate the occurrence of TIDs in the Asian sector during the storm using detrended TEC maps over Japan produced with a 15-min running window. The detrended TEC maps are available at the National Institute of Information and Communications Technology in Japan (https://aer-nc-web.nict.go.jp/GPS/GEONET). The maps have a spatial resolution of  $1.35^{\circ} \times 1.35^{\circ}$  in longitude and latitude, and a temporal resolution of 10 min.

The TEC data over the United States are produced by the Massachusetts Institute of Technology Haystack Observatory (http://openmadrigal.org; Zhang et al., 2017). We use absolute TEC maps derived using the Madrigal line-of-sight data which come with a 15 s sampling rate and a 15° elevation cutoff for the investigation of the evolution of a TEC depletion band over the U.S. Detrended TEC maps with 1 min cadence are produced with a 15-min running window to assess the development of TIDs.

#### 3. Results and Discussion

The dynamic pressure of the solar wind and magnetic indices on 25–26 August 2018 are presented in Figure 1a. Time progresses from right to left in order to match the westward progression of the Swarm orbits shown in Figures 1b and 1c. Following the southward turning of the interplantery magnetic field (IMF), currents on the auroral oval and ring current increase as the SME (SuperMAG electrojet) index and SYM-H indices indicate. SME is the generalization of the traditional auroral electrojet index to include more than 100 magnetometer stations (Gjerloev, 2012; Newell & Gjerloev, 2011a, 2011b).

The observations of Swarm satellites provide an overview of the spatial distribution of irregularities during the storm. The orbits and observations of Swarm-B at 21.5 hr LT and of Swarm-C at 2.5 hr LT are illustrated in Figures 1b and 1c, respectively. The times of the descending node of Swarm-B and the ascending node of Swarm-C are indicated by the vertical blue and black lines, respectively, in the SYM-H plot in Figure 1a. The thick red lines in the Swarm orbits indicate the detection locations of irregularities in the plasma density. Longitudes can

CHANG ET AL. 2 of 11



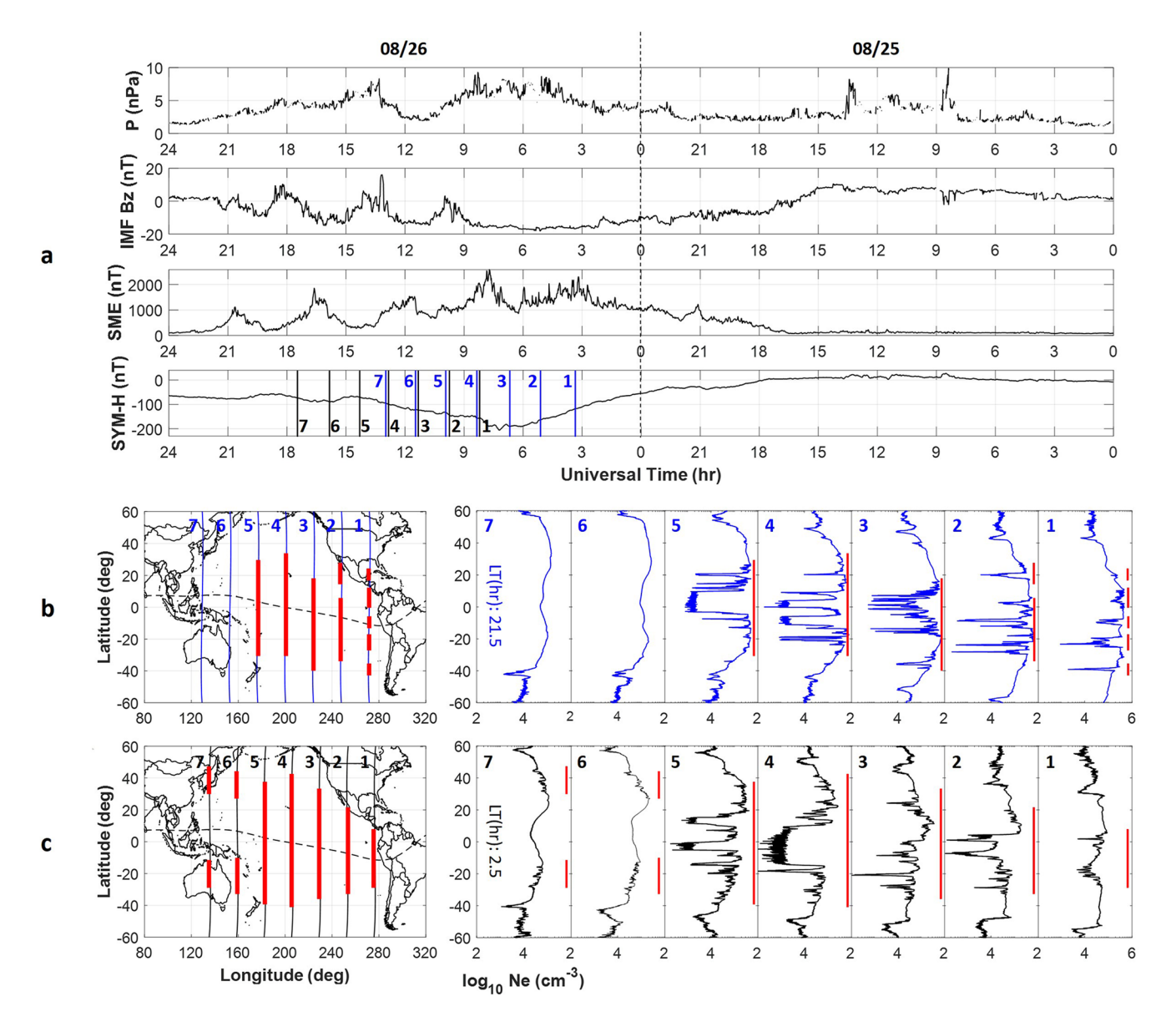


Figure 1. Overview of ionospheric disturbances in low and midlatitudes during the geomagnetic storm on 26 August 2018. (a) Solar wind dynamic pressure, interplanetary magnetic field (IMF) Bz component, SuperMAG electrojet (SME) index, and SYM-H index from the top to the bottom. The times of the descending nodes of Swarm-B and ascending nodes of Swarm-C orbits are indicated by blue and black lines, respectively, in the SYM-H plot. (b) Orbits of Swarm-B and measurements of the electron density along the orbits. (c) Orbits of Swarm-C and measurements of the electron density along the orbits. The red thick lines in Swarm orbits indicate the detection locations of irregularities. The local times (LTs) of Swarm-B and Swarm-C orbits are 21.5 and 2.5 hr, respectively.

be demarcated into two sectors based on the occurrence of irregularities in the equatorial region. EPBs are detected in the equatorial region of the Pacific sector (orbits 1–5), whereas they are absent in the equatorial region of the Asian sector (orbits 6 and 7). In the Asian sector, irregularities are absent from the equatorial region to midlatitudes at pre-midnight (Figure 1b). At post-midnight (Figure 1c), irregularities appear only at midlatitudes. Therefore, the midlatitude irregularities in the Asian sector are not related to EPBs. In the Pacific sector, Swarm-B observations reveal the development of intense EPBs in the equatorial region at pre-midnight. The comparison of the Swarm-B and Swarm-C observations in orbits 3–5 reveals the development of more intense plasma depletions at post-midnight than at pre-midnight in midlatitudes. The broad depletions near the magnetic equator in Swarm-B orbit 5 and Swarm-C orbit 4 are interpreted in terms of the uplift of the *F* peak height over the Swarm orbits. Midlatitude irregularities in the Pacific sector may be interpreted in terms of EPBs because

CHANG ET AL. 3 of 11



severe plasma depletions occur in the equatorial region. However, as revealed by observations in the Asian sector, the development of midlatitude depletions is not contingent with the occurrence of EPBs.

Ionospheric perturbations in low and midlatitudes during geomagnetic storms are closely related to the external energy deposition into the polar atmosphere. The heating of the atmosphere over the auroral oval by intense electric fields, energetic particle precipitation, and ion–neutral collisions modifies the global wind circulation pattern, produces neutral composition disturbances, and launches large-scale traveling atmospheric disturbances. In addition, the effect of external electric fields driven by solar winds or magnetospheric plasma convection extends to equatorial latitudes (Huang, 2008; Jaggi & Wolf, 1973; Kelley et al., 1979; Kikuchi, 2021; Nishida, 1968; Nopper & Carovillano, 1978). Ionospheric disturbances during geomagnetic storms result from the combination of these and other complex physical processes in the magnetosphere—thermosphere—ionosphere system. Severe ionospheric uplift is often observed in the equatorial region, in association with penetration electric fields during the main phase of geomagnetic storms (Kil et al., 2007). Midlatitude depletions detected on 26 August 2018 can be attributed to the development of large EPBs by the severe uplift. However, traveling atmospheric disturbances launched from the auroral region also promote the development of intense TIDs in midlatitudes (Nishioka et al., 2009; Tsugawa et al., 2004; Zhang et al., 2019), and midlatitude depletions can be produced by polarization electric fields in TIDs. In the following sections, we further examine ionospheric conditions using DMSP observations and TEC maps.

#### 3.1. Observations in the Asian Sector

The Swarm observations in the Asian sector indicate that plasma depletions can develop locally in midlatitudes in the absence of EPBs. We further support this interpretation by using the observations of the DMSP and TEC maps over Japan. The orbits and observations of DMSP F15 and F16 in the Asian sector are presented in Figure 2a. The LTs of F15 and F16 at the descending nodes are 2.9 and 3.8 hr, respectively. Irregularities were detected at the locations indicated by thick green lines. The morphologies of the midlatitude irregularities in the four DMSP orbits are similar, and the DMSP observations are similar to the Swarm-C observations depicted in Figure 1c. Many irregularities in midlatitudes appear as plasma depletions and can be interpreted as EPBs. The formation of the equatorial ionization trough at the altitude of the DMSP indicates the occurrence of ionospheric uplift in the region. Despite the ionosphere uplift, EPBs were not observed throughout the night.

The Swarm-C and DMSP observations in the Asian sector reveal the development of similar irregularities at the magnetic conjugate locations. These observations are consistent with the conjugate property of medium-scale TIDs (MSTIDs; Martinis et al., 2011, 2019; Otsuka et al., 2004; Shiokawa et al., 2005). Figure 2b illustrates the detrended TEC maps over Japan around the occurrence of DMSP orbits 3 and 4. The detrended TEC maps were produced by subtracting the background TEC using a 15-min running window. Although TEC perturbations reveal complex variations, the alignment of TEC perturbations in the northwest–southeast direction is dominant. This is a typical characteristic of MSTIDs in the Northern Hemisphere (Garcia et al., 2000; Martinis et al., 2010; Mendillo et al., 1997; Saito et al., 1998; Shiokawa et al., 2003). The TEC maps along with the Swarm and DMSP observations confirm the local development of plasma depletions at midlatitudes in association with TIDs.

#### 3.2. Observations in the Pacific Sector

As EPBs are absent in the equatorial region and TIDs are present at midlatitudes, the sources of midlatitude irregularities in the Asian sector can be easily assessed. In the Pacific sector, we cannot determine the sources of midlatitude irregularities because TID information is not available for the area over the ocean. Even if we identify the development of TIDs in this region, midlatitude irregularities associated with EPBs and TIDs are not distinguishable from satellite data. Although we cannot clarify the identity of midlatitude irregularities with our data set, we highlight certain aspects that may provide clues for the role of EPBs. By comparing the Swarm-B, Swarm-C, F16, and F17 observations at different LTs, we infer the temporal evolution of irregularities. In Figure 3, the observations around (a) 210°E and (b) 185°E are compared. The density plots are ordered from left to right following the order of LTs of satellites: Swarm-B (21.5 hr), Swarm-C (2.5 hr), DMSP-F16 (3.8 hr), and DMSP-F17 (6.6 hr).

Large density holes and deep ionization troughs occur in the equatorial region along different satellite orbits. These observations indicate the occurrence of severe ionospheric uplift over the Pacific Ocean. The difference

CHANG ET AL. 4 of 11



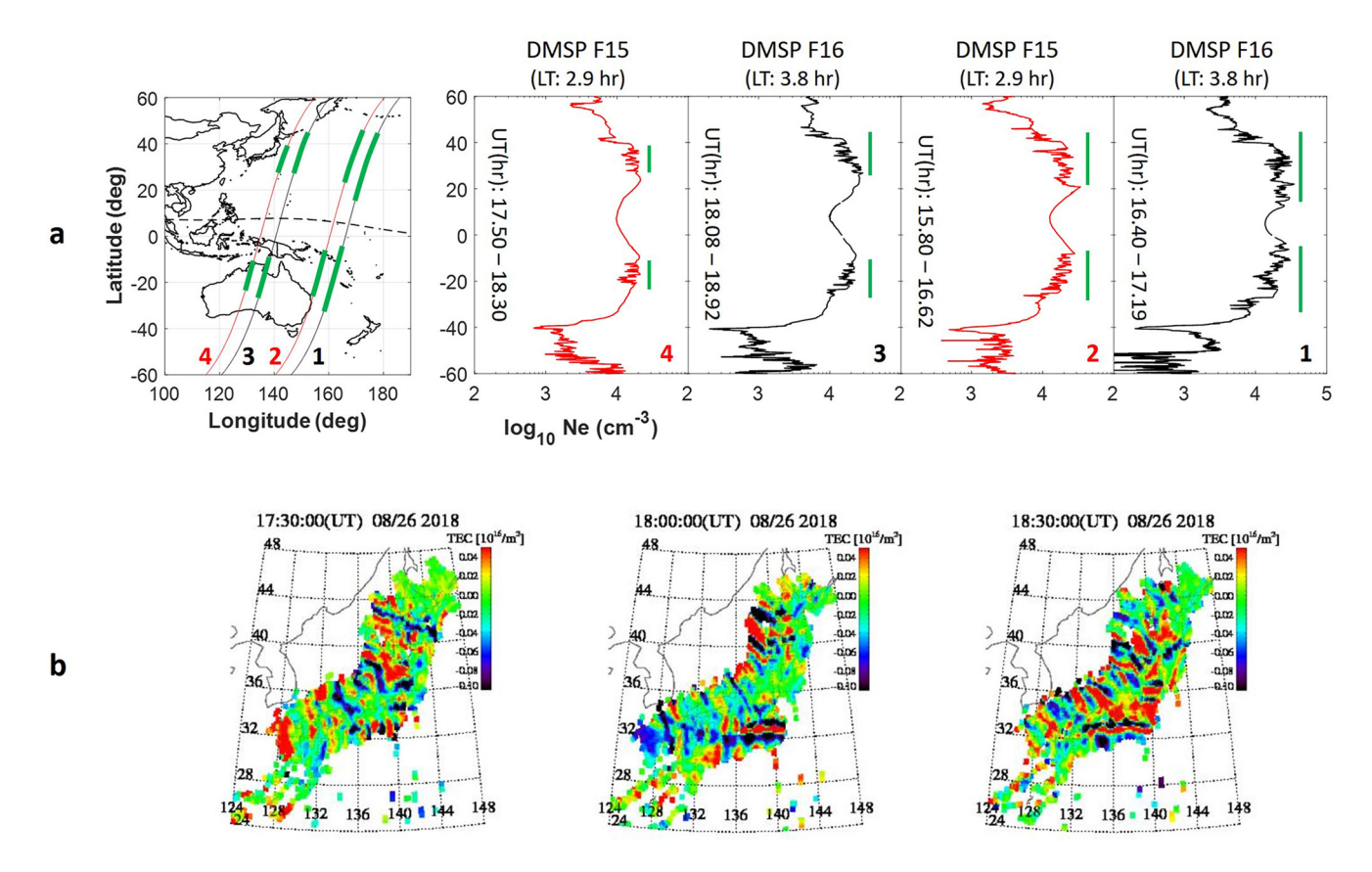


Figure 2. Defense Meteorological Satellite Program (DMSP) F15 and F16 observations in the Asian sector. The detection locations of irregularities are indicated by green thick lines in the orbits. The LTs at the descending nodes of F15 and F16 orbits are 2.9 and 3.8 hr, respectively. (b) Detrended total electron content (TEC) maps over Japan near the time periods of the DMSP orbits 3 and 4. The detrended TEC maps are derived using 15-min running window.

in the magnitudes of the density holes in various orbits reflects the variability of the uplift with longitude. In pre-midnight Swarm-B observations (Figures 3a and 3b), several intense plasma depletions appear within  $\pm 20^{\circ}$  latitudes, whereas only a few small depletions appear beyond  $\pm 20^{\circ}$  latitudes, wherein depletions are more pronounced in Swarm-C and F16 observations (post-midnight) than in Swarm-B observations (pre-midnight). Although the F16 observations were made 1.3 hr later in LT and 300 km higher altitude compared with the Swarm-C observations, the amplitudes of midlatitude plasma depletions in F16 observations are comparable or even greater than those in Swarm-C observations. F17 observations at 6.6 hr LT reveal the persistence of irregularities outside the equatorial region even after sunrise. A similar behavior of irregularities in the two longitudinal regions indicates the development of more intense midlatitude plasma depletions at post-midnight than at pre-midnight in the Pacific sector.

We can consider three scenarios to explain the behavior of midlatitude plasma depletions in the Pacific sector. First, the EPBs developed at pre-midnight may grow throughout the night and produce intense depletions at later LTs in midlatitudes. In general, EPBs rapidly grow within a few hours at pre-midnight as model simulations (Huba et al., 2008; Krall et al., 2010; Retterer, 2010; Zalesak & Ossakow, 1980) and the LT distribution of EPBs (Aa et al., 2020; Kil & Heelis, 1998b; Su et al., 2006) show. Compared to this typical behavior of pre-midnight EPBs, the growth of pre-midnight EPBs throughout the night is an anomalous behavior. Second, we can consider the development of new EPBs after midnight. However, this is also an anomalous behavior because no study has reported the development of new EPBs at post-midnight at the locations where EPBs were already developed at pre-midnight. The occurrence of these two scenarios under storm conditions cannot be ruled out, but, as a third scenario, we can consider the generation of midlatitude depletions by other sources. The morphology of midlatitude irregularities in the Pacific sector does not differ much from that associated with TIDs in the Asian sector. Therefore, midlatitude irregularities in the Pacific sector can be associated with the development of TIDs at post-midnight.

CHANG ET AL. 5 of 11



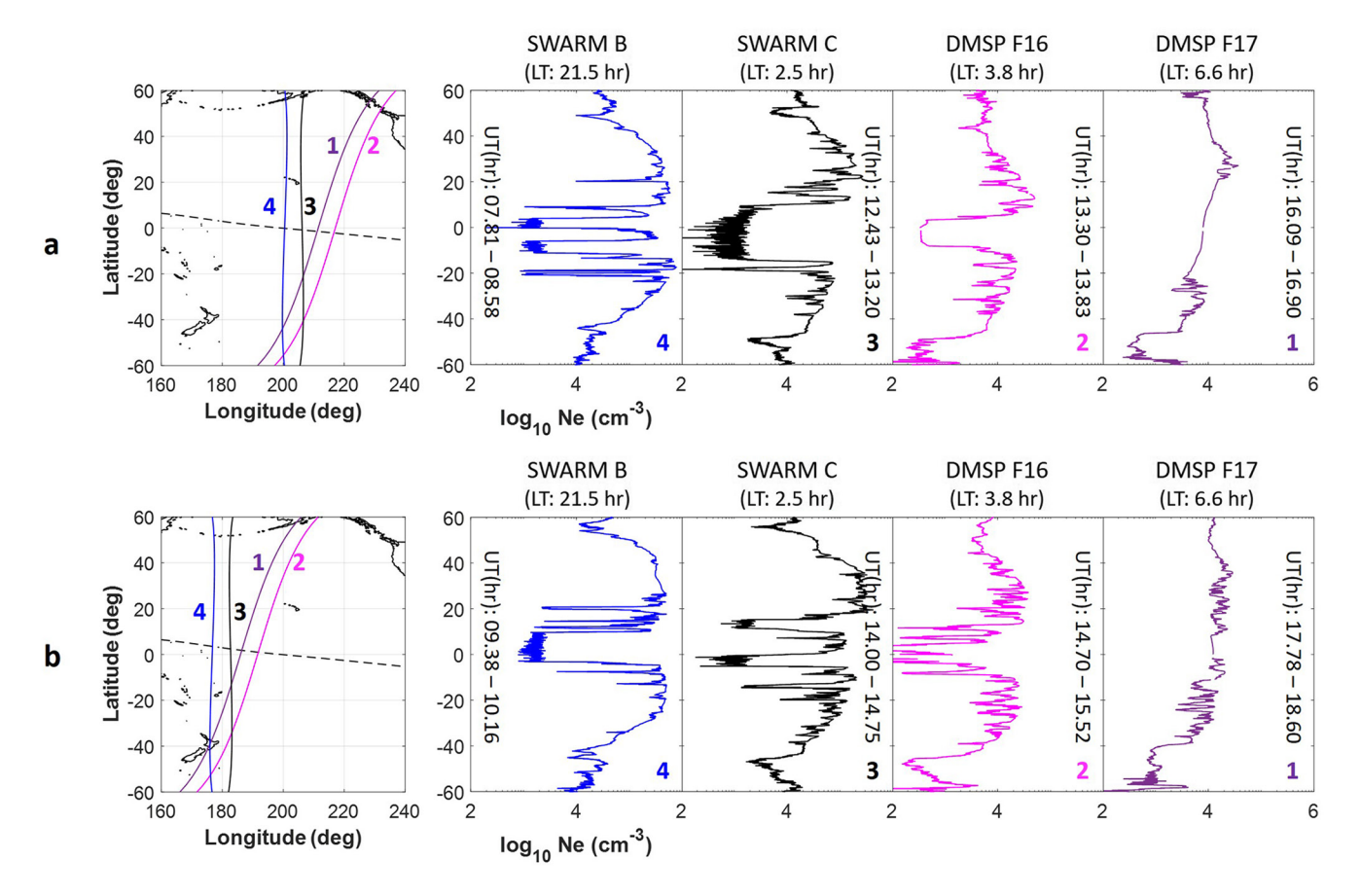


**Figure 3.** Comparison of Swarm and DMSP observations in the Pacific sector. The observations are divided into two regions near (a) 210°E and (b) 185°E longitudes. The LTs at the descending nodes of Swarm-B and DMSP and the ascending node of Swarm-C are Swarm-B (21.5 hr), Swarm-C (2.5 hr), DMSP-F16 (3.8 hr), and DMSP-F17 (6.6 hr). The density plots are ordered from left to right following the increasing order of the LTs.

Figure 3a illustrates an interesting feature of the F17 observations in formation of a flat density in the equatorial region. A smaller size of this phenomenon also appears in the F17 observations in Figure 3b. The formation of flat density in the equatorial region can be explained by the combined effect of ionospheric uplift and photoionization. As revealed by F16 observations, large ionization troughs are formed in the equatorial region before sunrise. Because the equatorial ionization trough, including EPBs, is quickly refilled in the morning by photoionization, the equatorial ionosphere reveals a latitudinally smooth density profile. The plasma refilling by photoionization is time consuming in the region with larger background plasma density. The persistence of irregularities outside the equatorial region in the F17 observations is attributed to the larger background density.

#### 3.3. TEC Depletion Band in the U.S.

In this section, we discuss the identity of a TEC depletion band detected near the west coast of the U.S. TEC depletion in this structure is significant, as it is clearly visible from absolute TEC maps. Figure 4 illustrates the absolute TEC maps produced using TEC data for 5 min. The TEC depletion band is indicated by red arrows. This structure emerges around 04:30 UT, intensifies with time, and moves westward. Because the severity of TEC depletion within the TEC depletion band varies with time and as TEC data present gaps over the ocean, it is difficult to determine the movement of the TEC depletion band in the north–south direction. In the present study, we investigate whether the TEC depletion band is a local midlatitude phenomenon or is associated with an EPB. If the TEC depletion band was produced by an EPB, it would be extended to low latitudes. However, the equatorward extension of the TEC depletion band is not evident in the TEC maps.

We further assess the evolution of the TEC depletion band using the keograms illustrated in Figure 5. Two keograms at 35°N and 30°N are produced using the absolute TEC data in 35°–35.5°N and 30°–30.5°N, respectively,

CHANG ET AL. 6 of 11

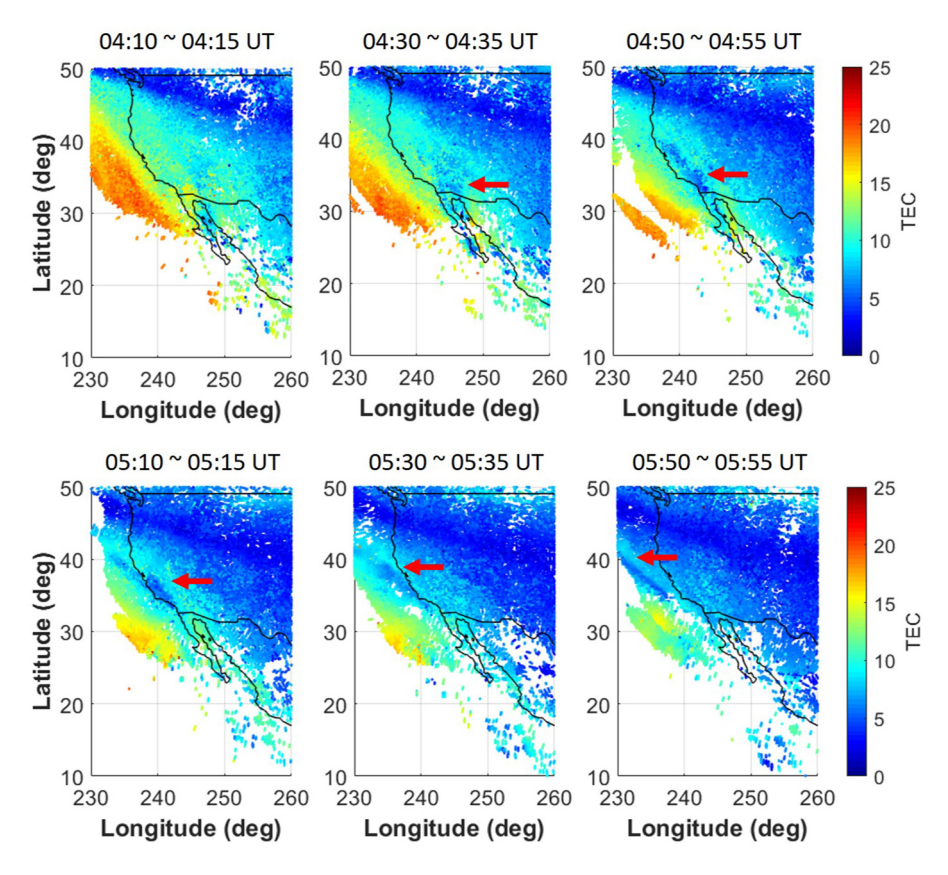


**Figure 4.** Evolution of a TEC depletion band at west coast of the U.S. Absolute TEC maps are produced using the TEC data for 5 min. The TEC depletion band is indicated by red arrows.

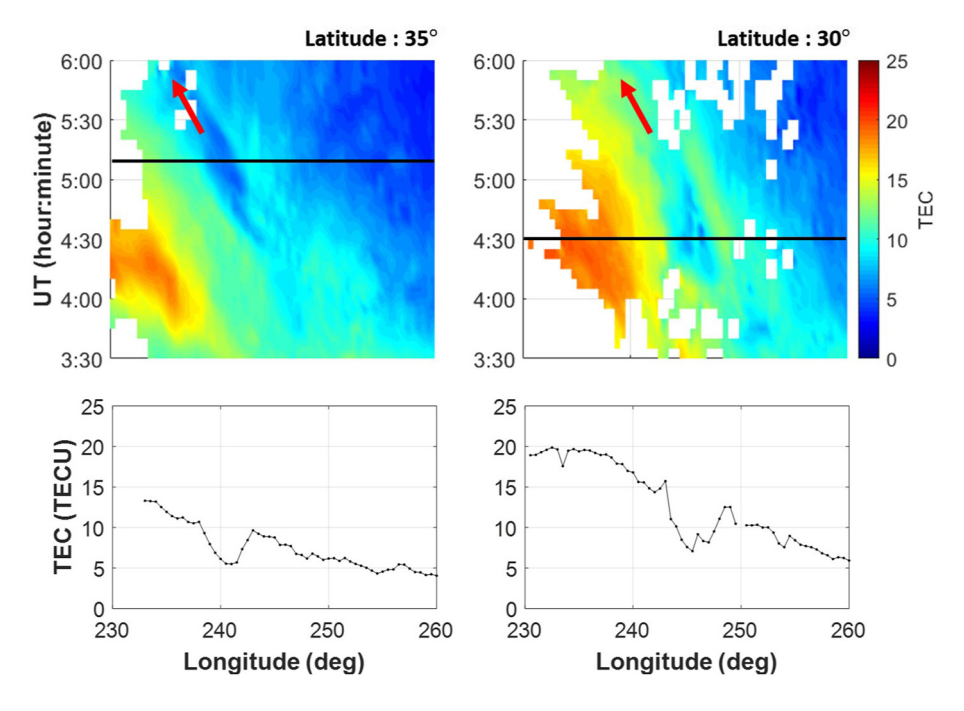


Figure 5. Keograms of absolute TEC at  $35^{\circ}N$  and  $30^{\circ}N$  latitudes. The TEC data along the black lines in the keograms are depicted at the bottom of the keograms.

CHANG ET AL. 7 of 11

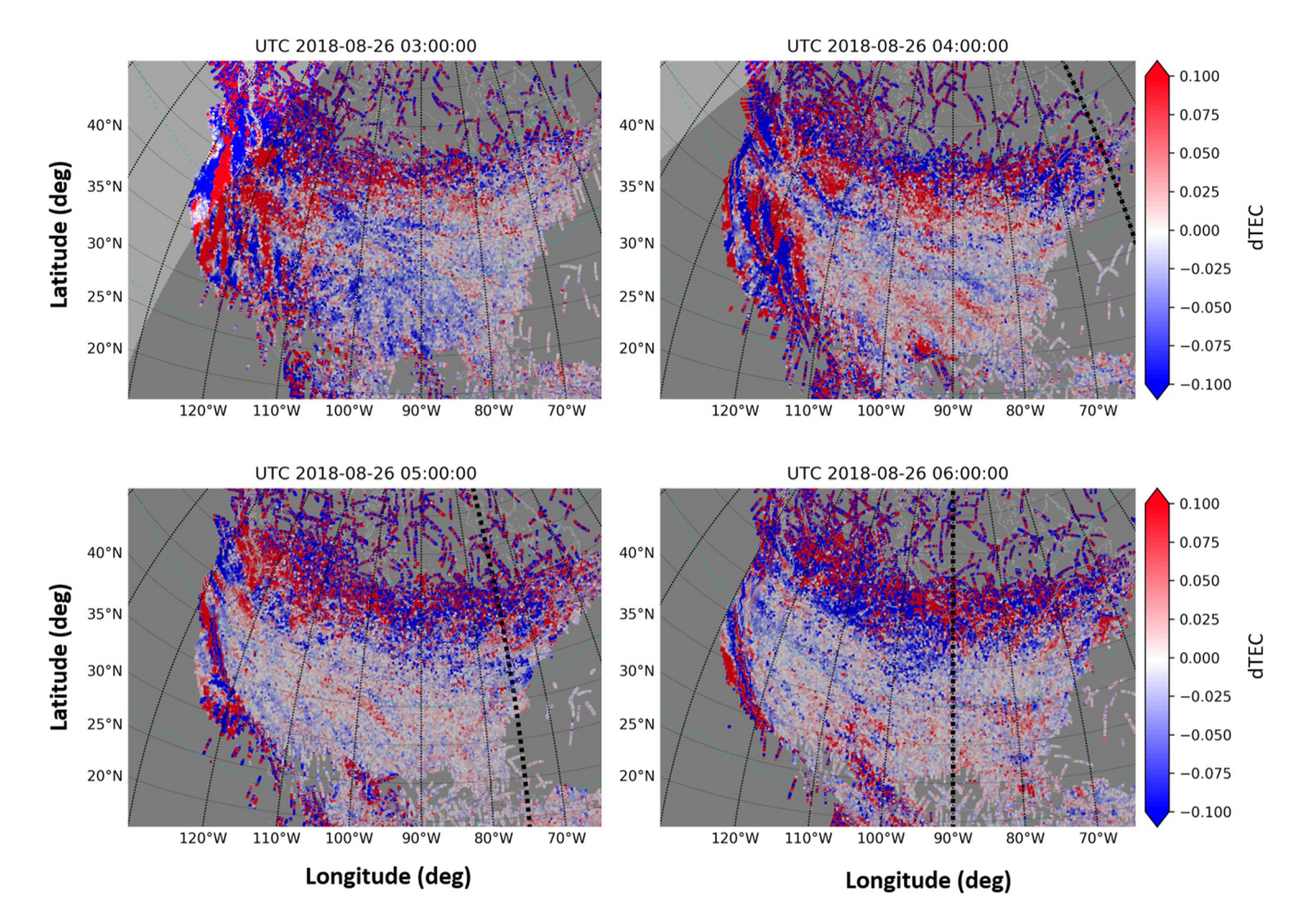


Figure 6. Detrended TEC maps at 03:00, 04:00, 05:00, and 06:00 UTs. The detrended TEC maps are produced using a 15-min running window. Day and night sides are distinguished by light and dark gray shadows, and black dotted lines demarcate midnight.

and by binning the data in  $0.5^{\circ} \times 5$  min longitude and UT bins. The red arrows indicate the direction of TEC depletion band movement. The westward velocity of the TEC depletion band estimated from the keograms was approximately 240 m/s. The TEC values along the black lines are depicted at the bottom of the keograms. Approximately 5 TEC units (1 TECU =  $10^{16}$  m<sup>-2</sup>) depletion is observed in the TEC depletion band. The keograms reveal different temporal variations of the TEC depletion band at 35°N and 30°N. TEC depletion intensifies with time at 35°N, whereas TEC depletion reduces with time at 30°N (Figure 4). The duration of TEC depletion at both latitudes is approximately 2 hr. If the TEC depletion band is the signature of an EPB, then the keograms indicate the growth of the EPB with time at higher latitudes (altitudes) and its decay at lower latitudes (altitudes). This behavior is inconsistent to the normal morphology of EPBs identified by other observations. In radar observations, EPBs appear as plumes by the vertical extension of plasma depletion from the bottomside of the F region to the upper bound of EPBs (Kelley et al., 1981; Woodman & La Hoz, 1976). In optical observations from space, EPBs appear as reversed C-shaped bands (Kelley et al., 2003; Kil et al., 2004, 2009). If EPBs decay faster at lower altitudes (latitudes), then they would appear as isolated structures instead of plume structures or reversed C-shaped bands. Based on the keograms and TEC maps in Figure 4, the TEC depletion band is interpreted as a local structure at midlatitudes.

Excluding EPBs from the source, TID presumably acts as a source of the TEC depletion band. The alignment of the TEC depletion band in the northwest–southeast direction and westward movement are consistent with the characteristics of MSTIDs. We examine the development of TIDs using detrended TEC maps over North America. The detrended TEC maps in Figure 6 are produced using a 15-min running window. TEC perturbations are confined to the western U.S. during the storm. Individual TEC perturbations are difficult to trace due to rapid

CHANG ET AL. 8 of 11



variation in perturbations. This situation is similar to the detrended TEC maps in Japan. However, the common feature in the western U.S. is the alignment of perturbations in the northwest-southeast direction and their movement toward the west. Therefore, the TEC depletion band is considered to be a component of the TIDs in this region. Storm-induced electric fields, for example, the polarward electric field associated with the subauroral polarization stream often observed over the continental US (Zhang et al., 2019) and penetration eastward electric field causing ionospheric uplift (Nishioka et al., 2009), and/or disturbance neutral wind dynamo may intensify the Perkins instability (Perkins, 1973) and locally produce deep plasma depletion. This interpretation needs to be validated by model simulations.

#### 4. Conclusions

We investigate the ionospheric disturbances at low and midlatitudes during the geomagnetic storm on 26 August 2018, thereby focusing on the identity of plasma depletions at midlatitudes. In the Asian sector, Swarm and DMSP satellites detected plasma depletions at midlatitudes in the absence of EPBs in the equatorial region. The MSTID features over Japan in TEC maps support the association of midlatitude plasma depletions in the Asian sector with TIDs. The TEC depletion band observed on the west coast of the U.S. is also interpreted in association with TIDs. These observations provide strong evidence that plasma depletion can be produced by local sources at midlatitudes. Because EPB is not a unique source of midlatitude plasma depletion, the morphology of midlatitude irregularities and their cooccurrence with EPBs do not provide strong evidence of the role of EPBs in the generation of midlatitude plasma depletions.

#### **Data Availability Statement**

The pressure, IMF Bz, and SYM-H data are from the OMNI Web Data Explorer system through the website (https://omniweb.gsfc.nasa.gov/form/omni\_min.html). The SME index is available from the SuperMAG website (http://supermag.jhuapl.edu/indices). The DMSP F15, F16, and F17 data are available from the CEDAR Madrigal database website (http://cedar.openmadrigal.org/ftp/). Swarm data are available on the ESA website (https:// earth.esa.int/web/guest/missions/esa-operational-eo-missions/swarm). The detrended TEC maps in Figure 2b are available on the NICT website (https://aer-nc-web.nict.go.jp/GPS/DRAWING-TEC/). The US TEC data are from the Madrigal database (http://cedar.openmadrigal.org/openmadrigal/). Original data for TEC processing are provided by the following organizations: UNAVCO, SOPAC, IGN (France), IGS, CDDIS, NGS, IBGE (Brazil), RAMSAC (Argentina), CORS (Panama), Arecibo Observatory, LISN, Topcon, CHAIN (Canada), CRS (Italy), SONEL, RENAG (New Zealand), GNSS Reference Networks, Finnish Meteorological Institute, and SWEPOS.

from Korea Astronomy and Space Science Institute (No. 2021-1-8-5012). A. K. Sun received support from the Space International Cooperation Program of the National Research Foundation (NRF) funded by the Korean Ministry of Science and ICT (NRF-2019M1A-3B2A0410271412). J. Lee acknowledges support from the MSIT (Ministry of Science, ICT), Korea, under the High-Potential Individuals Global Training Program (No. 2020-0-01531) supervised by the Institute for Information & Communications Technology Planning & Evaluation (IITP). H. Kil acknowledges support from NSF-AGS2029840. Air Force MURI FA9559-16-1-0364, and AOARD FA2386-21-1-4034. S.-R. Zhang received funding support from the Air Force MURI grant FA9559-16-1-0364, NSF grant AGS-2033787, and NASA LWS grant 80NSSC19K0078. GPS TEC data products and access through the Madrigal distributed data system were provided to the community (http://www.openmadrigal.org) by the Massachusetts Institute of Technology (MIT) under the support of the U.S. National Science Foundation (NSF) grant AGS-1762141.

Acknowledgments

H. Chang received basic research fund

#### References

- Aa, E., Huang, W., Liu, S., Ridley, A., Zou, S., & Shi, L. (2018). Midlatitude plasma bubbles over China and adjacent areas during a magnetic storm on 8 September 2017. Space Weather, 16, 321-331. https://doi.org/10.1002/2017SW001776
- Aa, E., Zou, S., & Liu, S. (2020). Statistical analysis of equatorial plasma irregularities retrieved from Swarm 2013-2019 observations. Journal of Geophysical Research: Space Physics, 125, e2019JA027022. https://doi.org/10.1029/2019JA027022
- Aa, E., Zou, S., Ridley, A., Zhang, S.-R., Coster, A. J., Erickson, P. J., et al. (2019). Merging of storm time midlatitude traveling ionospheric disturbances and equatorial plasma bubbles. Space Weather, 17, 285-298. https://doi.org/10.1029/2018SW002101
- Cherniak, I., & Zakharenkova, I. (2016). First observations of super plasma bubbles in Europe. Geophysical Research Letters, 43, 11137–11145. https://doi.org/10.1002/2016GL071421
- Cherniak, I., Zakharenkova, I., & Sokolovsky, S. (2019). Multi-instrumental observation of storm-induced ionospheric plasma bubbles at equatorial and middle latitudes. Journal of Geophysical Research: Space Physics, 124, 1491-1508. https://doi.org/10.1029/2018JA026309
- Garcia, F. J., Kelley, M. C., Makela, J. J., & Huang, C.-S. (2000). Airglow observations of mesoscale low-velocity traveling ionospheric disturbances at midlatitudes. Journal of Geophysical Research, 105, 18407-18415. https://doi.org/10.1029/1999JA000305
- Gjerloev, J. W. (2012). The SuperMAG data processing technique. Journal of Geophysical Research, 117, A09213. https://doi. org/10.1029/2012JA017683
- Huang, C.-S. (2008). Continuous penetration of the interplanetary electric field to the equatorial ionosphere over eight hours during intense geomagnetic storms. Journal of Geophysical Research, 113, A11305. https://doi.org/10.1029/2008JA013588
- Huang, C.-S., Foster, J. C., & Sahai, Y. (2007). Significant depletions of the ionospheric plasma density at middle latitudes: A possible signature of equatorial spread F bubbles near the plasmapause. Journal of Geophysical Research, 112, A05315. https://doi.org/10.1029/2007JA012307 Huba, J. D., Joyce, G., & Krall, J. (2008). Three-dimensional equatorial spread F modeling. Geophysical Research Letters, 35, L10102. https:// doi.org/10.1029/2008GL033509
- Jaggi, R. K., & Wolf, R. A. (1973). Self-consistent calculation of the motion of a sheet of ions in the magnetosphere. Journal of Geophysical Research, 78, 2852–2866. https://doi.org/10.1029/JA078i016p02852
- Kelley, M. C., Fejer, B. G., & Gonzales, C. A. (1979). An explanation for anomalous equatorial ionospheric electric field associated with a northward turning of the interplanetary magnetic field. Geophysical Research Letters, 6, 301-304. https://doi.org/10.1029/GL006i004p00301

CHANG ET AL. 9 of 11



- Kelley, M. C., Larsen, M. F., LaHoz, C., & McClure, J. P. (1981). Gravity wave initiation of equatorial spread F: A case study. *Journal of Geo-physical Research*, 86, 9087–9100. https://doi.org/10.1029/JA086iA11p09087
- Kelley, M. C., Makela, J. J., Paxton, L. J., Kamalabadi, F., Comberiate, J. M., & Kil, H. (2003). The first coordinated ground- and space-based optical observations of equatorial plasma bubbles. *Geophysical Research Letters*, 30(14), 1766. https://doi.org/10.1029/2003GL017301
- Kikuchi, T. (2021). Penetration of the magnetospheric electric fields to the low latitude ionosphere. Geographical Monograph Series, 315–338. https://doi.org/10.1002/9781119815617.ch14
- Kil, H., & Heelis, R. A. (1998a). Equatorial density irregularity structures at intermediate scales and their temporal evolution. *Journal of Geo-physical Research*, 103, 3969–3981. https://doi.org/10.1029/97JA03344
- Kil, H., & Heelis, R. A. (1998b). Global distribution of density irregularities in the equatorial ionosphere. *Journal of Geophysical Research*, 103, 407–417. https://doi.org/10.1029/97JA02698
- Kil, H., Heelis, R. A., Paxton, L. J., & Oh, S.-J. (2009). Formation of a plasma depletion shell in the equatorial ionosphere. *Journal of Geophysical Research*, 114, A11302. https://doi.org/10.1029/2009JA014369
- Kil, H., Lee, W. K., & Paxton, L. J. (2020). Origin and distribution of daytime electron density irregularities in the low-latitude F region. Journal of Geophysical Research: Space Physics, 125, e2020JA028343. https://doi.org/10.1029/2020JA028343
- Kil, H., Miller, E. S., Jee, G., Kwak, Y.-S., Zhang, Y., & Nishioka, M. (2016). Comment on "The night when the auroral and equatorial ionospheres converged" by Martinis, C., J. Baumgardner, M. Mendillo, J. Wroten, A. Coster, and L. Paxton. *Journal of Geophysical Research: Space Physics*, 121, 10599–10607. https://doi.org/10.1002/2016JA022662
- Kil, H., Oh, S.-J., Paxton, L. J., Zhang, Y., Su, S.-Y., & Min, K.-W. (2007). Spike-like change of the vertical  $\mathbf{E} \times \mathbf{B}$  drift in the equatorial region during very large geomagnetic storms. *Geophysical Research Letters*, 34, L09103. https://doi.org/10.1029/2007GL029277
- Kil, H., & Paxton, L. J. (2017). Global distribution of nighttime medium-scale traveling ionospheric disturbances seen by Swarm satellites. Geo-physical Research Letters, 44, 9176–9182. https://doi.org/10.1002/2017GL074750
- Kil, H., Su, S.-Y., Paxton, L. J., Wolven, B. C., Zhang, Y., Morrison, D., & Yeh, H. C. (2004). Coincident equatorial bubble detection by TIMED/GUVI and ROCSAT-1. Geophysical Research Letters, 31, L03809. https://doi.org/10.1029/2003GL018696
- Krall, J., Huba, J. D., Ossakow, S. L., & Joyce, G. (2010). Why do equatorial ionospheric bubbles stop rising? Geophysical Research Letters, 37, L09105. https://doi.org/10.1029/2010GL043128
- Lee, W. K., Kil, H., & Paxton, L. J. (2021). Global distribution of nighttime MSTIDs and its association with E region irregularities seen by CHAMP satellite. *Journal of Geophysical Research: Space Physics*, 126, e2020JA028836. https://doi.org/10.1029/2020JA028836
- Ma, G., & Maruyama, T. (2006). A super bubble detected by dense GPS network at east Asian longitudes. Geophysical Research Letters, 33, L21103. https://doi.org/10.1029/2006GL027512
- Martinis, C., Baumgardner, J., Mendillo, M., Wroten, J., Coster, A., & Paxton, L. (2015). The night when the auroral and equatorial ionospheres converged. *Journal of Geophysical Research: Space Physics*, 120, 8085–8095. https://doi.org/10.1002/2015JA021555
- Martinis, C., Baumgardner, J., Mendillo, M., Wroten, J., MacDonald, T., Kosch, M., et al. (2019). First conjugate observations of medium-scale traveling ionospheric disturbances (MSTIDs) in the Europe–Africa longitude sector. *Journal of Geophysical Research: Space Physics*, 124, 2213–2222. https://doi.org/10.1029/2018JA026018
- Martinis, C., Baumgardner, J., Wroten, J., & Mendillo, M. (2010). Seasonal dependence of MSTIDs obtained from 630.0 nm airglow imaging at Arecibo. *Geophysical Research Letters*, 37, L11103. https://doi.org/10.1029/2010GL043569
- Martinis, C., Baumgardner, J., Wroten, J., & Mendillo, M. (2011). All-sky imaging observations of conjugate medium-scale traveling ionospheric disturbances in the American sector. *Journal of Geophysical Research*, 116, A05326. https://doi.org/10.1029/2010JA016264
- Mendillo, M., Baumgardner, J., Nottingham, D., Aarons, J., Reinisch, B., Scali, J., & Kelley, M. (1997). Investigations of thermospheric-ion-ospheric dynamics with 6300-Å images from the Arecibo Observatory. *Journal of Geophysical Research*, 102, 7331–7343. https://doi.org/10.1029/96JA02786
- Mendillo, M., Zesta, E., Shodhan, S., Sultan, P. J., Doe, R., Sahai, Y., & Baumgardner, J. (2005). Observations and modeling of the coupled latitude–altitude patterns of equatorial plasma depletions. *Journal of Geophysical Research*, 110, A09303. https://doi.org/10.1029/2005JA011157
- Miller, E. S., Makela, J. J., & Kelley, M. C. (2009). Seeding of equatorial plasma depletions by polarization electric fields from middle latitudes: Experimental evidence. *Geophysical Research Letters*, 36, L18105. https://doi.org/10.1029/2009GL039695
- Newell, P. T., & Gjerloev, J. W. (2011a). Evaluation of SuperMAG auroral electrojet indices as indicators of substorms and auroral power. *Journal of Geophysical Research*, 116, A12211. https://doi.org/10.1029/2011JA016779
- Newell, P. T., & Gjerloev, J. W. (2011b). Substorm and magnetosphere characteristic scales inferred from the SuperMAG auroral electrojet indi-
- ces. Journal of Geophysical Research, 116, A12232. https://doi.org/10.1029/2011JA016936

  Nishida, A. (1968). Coherence of geomagnetic DP 2 fluctuations with interplanetary magnetic variations. Journal of Geophysical Research, 73,
- Nishioka, M., Saito, A., & Tsugawa, T. (2008). Occurrence characteristics of plasma bubble derived from global ground-based GPS receiver networks. *Journal of Geophysical Research*, 113, A05301. https://doi.org/10.1029/2007JA012605
- Nishioka, M., Saito, A., & Tsugawa, T. (2009). Super-medium-scale traveling ionospheric disturbance observed at midlatitude during the geomagnetic storm on 10 November 2004. Journal of Geophysical Research, 114, A07310. https://doi.org/10.1029/2008JA013581
- Nopper, R. W., & Carovillano, R. L. (1978). Polar-equatorial coupling during magnetically active periods. *Geophysical Research Letters*, 5, 699–702. https://doi.org/10.1029/GL005i008p00699
- Otsuka, Y., Shiokawa, K., & Ogawa, T. (2012). Disappearance of equatorial plasma bubble after interaction with mid-latitude medium-scale traveling ionospheric disturbance. *Geophysical Research Letters*, 39, L14105. https://doi.org/10.1029/2012GL052286
- Otsuka, Y., Shiokawa, K., Ogawa, T., & Wilkinson, P. (2004). Geomagnetic conjugate observations of medium-scale traveling ionospheric disturbances at midlatitude using all-sky airglow imagers. *Geophysical Research Letters*, 31, L15803. https://doi.org/10.1029/2004GL020262
- Park, J., Lühr, H., Min, K., & Lee, J. (2010). Plasma density undulations in the nighttime mid-latitude F-region as observed by CHAMP, KOMP-SAT-1 M, and DMSP F15. Journal of Atmospheric and Solar-Terrestrial Physics, 72, 183–192. https://doi.org/10.1016/j.jastp.2009.11.007
- Perkins, F. (1973). Spread F and ionospheric currents. *Journal of Geophysical Research*, 78, 218–226. https://doi.org/10.1029/JA078i001p00218
  Retterer, J. M. (2010). Forecasting low-latitude radio scintillation with 3-D ionospheric plume models: 1. Plume model. *Journal of Geophysical Research*, 115, A03306. https://doi.org/10.1029/2008JA013840
- Saito, A., Fukao, S., & Miyazaki, S. (1998). High resolution mapping of TEC perturbations with the GSI GPS network over Japans. *Geophysical Research Letters*, 25, 3079–3082. https://doi.org/10.1029/98GL52361
- Shiokawa, K., Ihara, C., Otsuka, Y., & Ogawa, T. (2003). Statistical study of nighttime medium-scale traveling ionospheric disturbances using midlatitude airglow images. *Journal of Geophysical Research*, 108(A1), 1052. https://doi.org/10.1029/2002JA009491

CHANG ET AL. 10 of 11

5549-5559. https://doi.org/10.1029/JA073i017p05549



- Shiokawa, K., Otsuka, Y., Tsugawa, T., Ogawa, T., Saito, A., Ohshima, K., et al. (2005). Geomagnetic conjugate observation of nighttime medium-scale and large-scale traveling ionospheric disturbances: FRONT3 campaign. *Journal of Geophysical Research*, 110, A05303. https://doi.org/10.1029/2004JA010845
- Su, S.-Y., Liu, C. H., Ho, H. H., & Chao, C. K. (2006). Distribution characteristics of topside ionospheric density irregularities: Equatorial versus midlatitude regions. *Journal of Geophysical Research*, 111, A06305. https://doi.org/10.1029/2005JA011330
- Takahashi, H., Wrasse, C. M., Figueiredo, C. A. O. B., Barros, D., Abdu, M. A., Otsuka, Y., & Shiokawa, K. (2018). Equatorial plasma bubble seeding by MSTIDs in the ionosphere. *Progress in Earth and Planetary Science*, 5, 32. https://doi.org/10.1186/s40645-018-0189-2
- Tsugawa, T., Saito, A., & Otsuka, Y. (2004). A statistical study of large-scale traveling ionospheric disturbances using the GPS network in Japan. Journal of Geophysical Research, 109, A06302. https://doi.org/10.1029/2003JA010302
- Woodman, R. F., & La Hoz, C. (1976). Radar observations of F region equatorial irregularities. Journal of Geophysical Research, 81, 5447–5466. https://doi.org/10.1029/JA081i031p05447
- Zakharenkova, I., & Cherniak, I. (2020). When plasma streams tie up equatorial plasma irregularities with auroral ones. Space Weather, 18, e2019SW002375. https://doi.org/10.1029/2019SW002375
- Zalesak, S. T., & Ossakow, S. L. (1980). Nonlinear equatorial spread F: Spatially large bubbles resulting from large horizontal scale initial perturbations. Journal of Geophysical Research, 85, 2131–2142. https://doi.org/10.1029/JA085iA05p02131
- Zhang, S.-R., Erickson, P. J., Coster, A. J., Rideout, W., Vierinen, J., Jonah, O., & Goncharenko, L. P. (2019). Subauroral and polar traveling ionospheric disturbances during the 7–9 September 2017 storms. Space Weather, 17, 1748–1764. https://doi.org/10.1029/2019SW002325
- Zhang, S.-R., Erickson, P. J., Goncharenko, L. P., Coster, A. J., Rideout, W., & Vierinen, J. (2017). Ionospheric bow waves and perturbations induced by the 21 August 2017 solar eclipse. *Geophysical Research Letters*, 44, 12067–12073. https://doi.org/10.1002/2017GL076054

CHANG ET AL. 11 of 11